Sensing in Electroanalysis

Vol. 7 (K. Kalcher, R. Metelka, I. Švancara, K. Vytřas; Eds.), pp. 9–28.

ISBN 978-80-7395-563-2 (printed); 978-80-7395-564-9 (on-line)

Microelectrode Arrays for Applications in Electrochemical Analysis

Vlastimil Rehacek[*], **Ivan Hotovy**, and **Marian Vojs**

Institute of Electronics and Photonics, Faculty of Electrical Enginnering and Information Technology Slovak University of Technology, Ilkovičova 3, 812 19 Bratislava, Slovakia

---

Abstract: The greater availability of microlithographic techniques for the fabrication of electrochemical devices has led to a significant increase in the development of microelectrodes and microelectrode arrays of various geometries with their excellent electrochemical properties. This paper is focused on theoretical aspects of microelectrodes and microelectrode arrays with loosely and densely spaced electrodes, their fabrication processes and electrochemical characterization. In this review, our attention is focused on microdisc electrode arrays and interdigitated array electrodes. Finally, selected examples are presented of the application of microelectrode arrays in environmental analysis.

Keywords: Microelectrode; Microelectrode array; Microdisc array; Interdigitated array electrodes; Mercury electrode; Bismuth film electrode; Diamond-like carbon; Boron-doped diamond; Voltammetric determination.

---

*) Author to whom correspondence should be addressed. E-mail: vlastimil.rehacek@stuba.sk

Introduction

Microelectrodes (MEs) and microelectrode arrays (MEAs) are very attractive for the research community. Their excellent analytical performance leads to the development of various electroanalytical applications in the field of electrochemistry, biotechnology, medicine and environmental science. MEAs have demonstrated to be powerful analytical tools for environmental analysis [1–3]. The unusual properties of MEs were discovered in the

1970s [1]. Compared to conventionally sized macroelectrodes (>1 mm), the ultramicro-electrodes possess a lot of features such as high mass transport due to radial diffusion, rapid attainment of the steady state, low ohmic drop, reduced non-faradaic charging current, small RC time constant, independency on convection and possibility to increase current responses with MEAs. Critical dimensions of MEs, in the order of some micrometers, make the electrochemical response differ from that of a conventional sized electrode and opens a new possibility for studying electrode reactions such as measurements in solutions with low electrolyte concentration, in non-polar solvents as well as in a solid or gas phase. Also the use of MEs in studying rapid homogenous or heterogeneous reactions is useful.

Equilibrium between diffusion of electroactive species to the electrode surface and the species that exchange electrons at this surface cannot be achieved in conventional sized electrodes. As a consequence, MEs can be applied in very fast scan-rate voltammetric measurements. An important feature of MEs is that their responses are independent of the convection of the solution. The small size of MEs makes possible in vivo investigations in neurological and physiological studies directly in bloodstream and living tissues or to measure in extremely small volumes of analytes. However, the excellent properties of MEs could be widely utilized since the developments in microelectronic technologies made it possible to reliably measure very low currents (in pA to nA range) and to fabricate micro- and submicrometer electrodes. MEs and MEAs are produced with various geometries (band, disc, ring, sphere, hemisphere, disc array, interdigitated array electrodes) (Fig. 1) of different materials (Au, Pt, Ir, C, Ag, *etc.*) and using various fabrication techniques (photolithography, screen printing, methods based on the dispersion of nanoparticles, mechanical methods, template methods, methods based on etching techniques) [1,3].

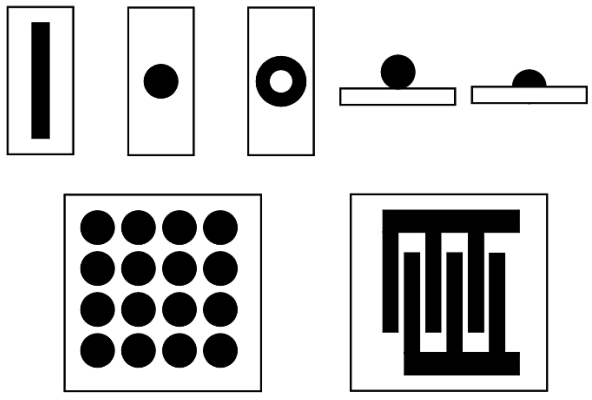

Fig. 1: *Microelectrodes and microelectrode arrays of various geometries.*

In this work, microelectrode arrays of various geometries (microdisc arrays (MDAs) and interdigitated array electrodes (IDAEs)) developed for electroanalysis of some inorganic pollutants are reviewed. This review summarizes, in addition to theoretical considerations, also microfabrication processes of MEAs by photolithography and their electrochemical characterization. Selected applications of MEAs in determination of different metal ions are described.

Theoretical Considerations

There are several definitions of a microelectrode (also the term ultramicroelectrode is used). One of them, the so-called geometrical definition, identifies a microelectrode as any electrode with at least one dimension not greater than 25 μm [4]. Other definitions [5–7] give a different value (20 μm) of the critical electrode dimension. From the point of view of microelectrode array behavior, more convenient is an operational definition of the microelectrode as any electrode whose characteristic dimension is, under given experimental conditions, comparable with or smaller than the diffusion layer thickness. Under these conditions, a steady-state or a pseudo steady-state is reached [8].

A microelectrode offers a number of attractive features in the field of electroanalysis over conventional macroelectrodes. The major advantageous feature of a microelectrode is its radial diffusion, which allows steady-state conditions to be reached rapidly in comparison with linear diffusion of a macroelectrode. It is known that the steady-state limiting current of a single microdisc electrode is proportional to the radius of the disc and is governed by equation [9] (1):

$$I_{lim} = 4nFDCr \qquad (1)$$

where n is the number of electrons involved in the electrochemical reaction, F is Faraday`s constant, D is the diffusion coefficient of the reactant, C is the bulk reactant concentration, and r is the electrode radius. For the microelectrode behavior a high mass transport is specific showing a sigmoidal cyclic voltammogram with a limiting current. Due to a reduced charging current and a small RC time constant, the voltammetric experiments can be performed at high scan rates. Extremely small currents and small ohmic drop allow to measure in high resistance solutions without a basic electrolyte as well as without a third auxiliary electrode. Thanks to

the reduced charging current, the ratio of faradaic-to-charging current (the smaller the electrode surface, the higher the measured signal-to-noise ratio) is improved and thereby the sensitivity can be higher. If the dimensions of the microelectrode are extremely small, the current response can be independent of the convection of the solution. On the other hand, the main drawback of a single microelectrode is its extremely small current which is difficult to measure.

Loosely Packed Microdisc Array

The most important benefit in using a microelectrode array is to enhance the measured currents considerably and, at the same time, to maintain the advantageous features of a single microelectrode. From the point of view of the spacing of the microelectrodes in the array there are two fundamental approaches how to arrange the MEs in an array. One of them considers a loosely packed array (interelectrode distance ≫ electrode size). This arrangement is typical for microdisc electrode arrays, which are the most frequently used in voltammetric measure. In comparison with a single microelectrode, the microelectrode array has to accomplish certain geometrical requirements in order to get a collective current response while maintaining the advantageous features of single microelectrodes. The most critical parameter is the interelectrode distance.

In the case of a microdisc array a minimum interelectrode distance has to be kept at least 10 times larger than the microdisc diameter [10,11]. If this requirement is satisfied, each microdisc behaves independently and the array provides characteristic advantages of a microelectrode. If the fabrication of the array by microlithography is based on the use of a thin insulating layer (polyimide, SiO_2, Si_3N_4, SiO_xN_y) with an array of openings on a conductive electrode layer, the thickness of the insulation layer is also important. An effect of a recessed microdisc on the electroanalytical response was reported [11, 12]. In comparison with an inlaid microelectrode array, the steady-state current was reduced by ~10% for a microdisc array with disc radius 5 μm and a 0.8 μm thick silicon nitride layer [12]. For an inlaid microdisc array, the steady-state limiting current proportional to both the microdisc radius and the number of microdisc electrodes was derived by Aoki et al. [11] (2):

$$I_{lim} = 4mnFDCr \qquad (2)$$

where m is the number of microdisc electrodes, n is the number of electrons involved in the electrochemical reaction, F is Faraday`s constant, D is the diffusion coefficient of the reactant, C is the bulk reactant concentration, and r is the electrode radius. In general, if the interelectrode distance is too small, the array behaves at voltammetric measurements as a single macroelectrode due to the so-called shielding effect caused by overlapping of the diffusion layers of adjacent discs.

Densely Packed Interdigitated Array Electrodes

On the other hand the MEAs with densely packed electrodes such as IDAEs are also attractive because of their microelectrode-like behavior, despite their relative large electrode area [13–16]. The IDA electrodes consist of a pair of microband finger electrodes that mesh with each other (see in Fig. 1). After the specific requirements are fulfilled (small distance between electrodes so that the diffusion layers of both electrodes overlap, electrochemical reversibility of the redox couples, each of the two electrodes potentiostated individually), the IDAEs can operate with the so-called redox cycling effect. In this case, the shielding effect caused by overlapping of the diffusion layers of the two finger electrodes is necessary. Reduced species generated at one electrode diffuse across a small gap to the adjacent electrode, where they are oxidized and diffuse back to the original electrode, creating process redox cycling. This cycling between two electrodes leads to a greatly amplified current.

It was found that if the interelectrode gap is smaller, the recycling current is higher. This phenomenon was first demonstrated by Bard et al. in 1986 [17]. The concept offers these advantages: steady-state current can be achieved in a very short time, the current can be improved more than 10 times by recycling the species, the signal-to-noise ratio can be enhanced due to the absence of a capacitive charging current at the collector electrode because its potential is fixed. Electrochemical measurements are carried out using a bipotentiostat. In dual-mode cyclic voltammetry one of the finger electrodes (collector electrode) is held at a fixed potential, while the other one (generator electrode) is swept in an appropriate potential range. The collector potential is set lower than the redox potential if the redox species in the solution are in reduced form.

The cycling effect is quantified by the redox cycling efficiency (or collection efficiency), which is defined as the ratio of the limiting collector current in the dual-mode to the limiting current in the single mode (collector electrode is not potentiostated). The cycling

efficiency increases if the dimensions of the electrodes and the interelectrode gap decrease. Of course, ions can diffuse out of the overlapping diffusion layer back into the bulk solution. If the dimensions of the electrode and the interelectrode gap are smaller, the probability that ions escape the diffusion layer is lower. Equation (3) was derived by Aoki et al. [18] for the limiting current that should flow in the IDAEs operating in the dual-mode:

$$| I_{lim}| = nFDCmb\left[0.637 \ln\left\{2.55(1+w_f/w_g)\right\} - 0.19/(1+w_f/w_g)^2\right] \quad (3)$$

From the point of view of construction of the IDAEs, the electrodes can be arranged horizontally or vertically [16]. Vertically ordered IDA electrodes have two advantages compared with ordinary planar IDAEs. First, the gap between the electrodes is easily controlled by the thickness of the insulation layer which can be thinner than the gap patterned horizontally by photolithography. Second, the total electrode area is smaller because the gap between the upper and lower electrodes acts as a vertical wall and reduces the total area.

Fabrication

Photolithography processes are generally used for the fabrication of MEAs of planar configuration even though they need expensive instrumentation. However, this technique provides very reliable and perfectly patterned geometric structures with submicrometric dimensions. Moreover, this technology allows mass production of low cost chips with MEAs on silicon wafers or alumina substrates in microelectronics industry.

Mercury Microdisc Array on Silicon Support

The silicon microelectrode array for mercury electroplating was fabricated very simply by the standard silicon technology (Fig. 2). The array consists of 50 625 silicon disc-shaped microelectrodes with disc diameter 2 μm each and interelectrode spacing 20 μm was patterned by photolithography on highly conductive (0.008–0.024 Ω·cm) p- or n-type silicon substrates. The mercury microdisc array was prepared by electrodeposition of mercury from a solution for ex-situ determination of Cd, Pb and Cu.

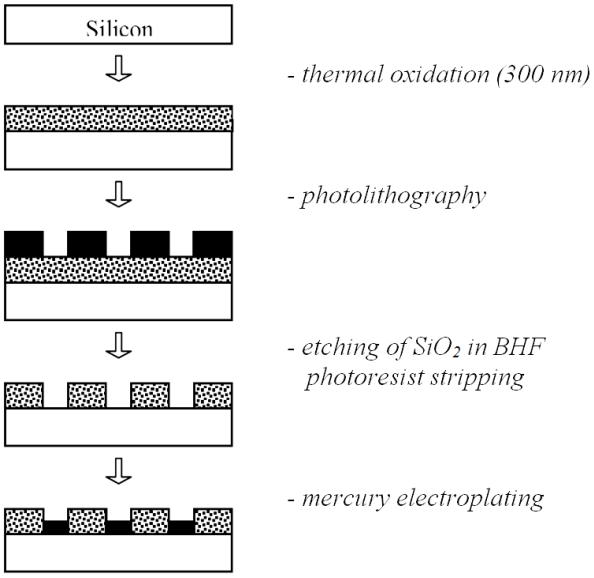

Fig. 2: *Fabrication process of the silicon based mercury MDA.*

Mercury (or Bismuth) Microdisc Array on Nitrogen-Doped Diamond-Like Carbon (NDDLC) Support

The nitrogen-doped DLC film was fabricated by vacuum pulse sputtering of graphite on a highly conductive silicon substrate. The areas which act as working electrodes (the array of microdiscs) were defined photolithographically using a positive photoresist with the same mask layout as already described. The cross-sectional view of the microelectrode array is shown in Fig. 3. The conductive supports were tested for in situ simultaneous determination of various metal ions (Cd, Pb and Cu) in mercury or bismuth film by anodic stripping voltammetry.

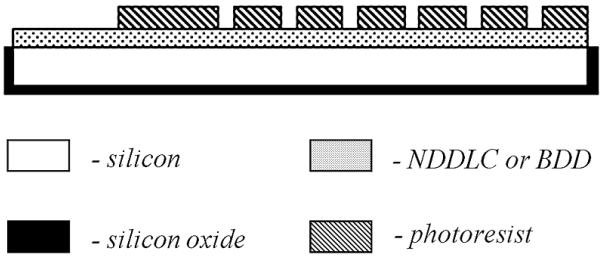

Fig. 3: *Cross-sectional view of the microelectrode array.*

Bismuth Microdisc Array on Boron-Doped Diamond (BDD) Support

The boron-doped diamond film was grown by microwave chemical vapor deposition (MWCVD) from methane diluted in hydrogen at substrate temperature 800 °C. Boron doping was achieved by adding trimethylboron (TMB) to the gas mixture at B:C ratio 6000 or 10 000 ppm in the gas phase. After deposition, the support was chemically cleaned in a strong oxidizing mixture of hot sulphuric acid with potassium nitride (at 200 °C for 30 min) followed by washing in deionized water. After the support was dried, the array of microdiscs was defined photolithographically using a positive photoresist (similar scheme as in Fig. 3). Fig. 4 shows a SEM image of the diamond morphology of BDD. Measurements with Raman spectroscopy of the diamond layers confirmed the diamond nature of these films. The grain size of 50 to 250 nm in BDD film was observed. The array was used for in-situ determination of Zn, Cd and Pb.

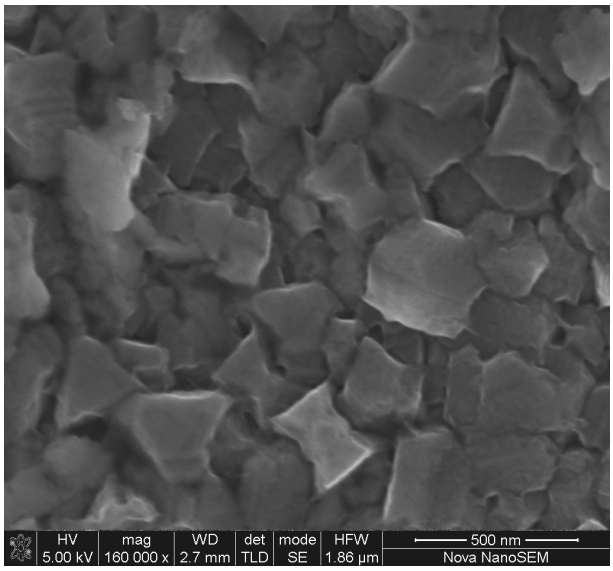

Fig. 4: *SEM image of surface of BDD.*

Platinum Interdigitated Array Electrode (IDAE) on Silicon/Silicon Dioxide Support

The vertically arranged IDA electrode with a bottom continuous Pt electrode and a middle insulation layer in the IDA form separating the upper Pt IDA electrodes was fabricated by r.f. sputtering, ion sputter/plasma etching, and photolithography with lift-off technique. The IDAE consisted of two series (26 pairs) of finger electrodes (see illustrative image in Fig. 5).

The finger widths and gaps were 5 μm and each finger was 400 μm long. In this vertical arrangement both upper electrodes form one array and the bottom Pt layer the second electrode, the gap between the arrays and bottom electrode is given by the thickness of the insulating layer (0.5 μm of Y_2O_3). Submicrometrically narrow vertical gap caused a significant increase of the diffusion layer overlap and thus increased the redox cycling current in comparison with horizontally spaced arrays. IDAE was used for determination of trace concentration of Fe in ultrapure spectral carbon as well as selenium in water samples.

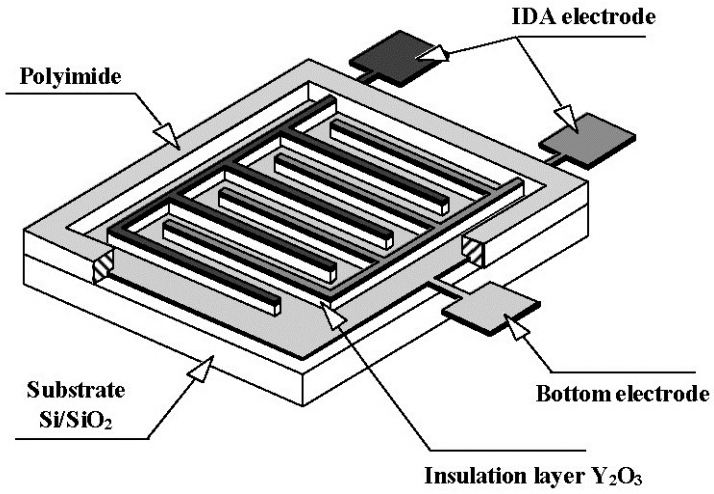

Fig. 5: *Schematic diagram of vertically arranged IDA electrode.*

Characterization

A method commonly used for characterization of microelectrodes and microelectrode arrays is cyclic voltammetry. The cyclic voltammetric behavior of microelectrode arrays is more complicated in comparison with single microelectrodes. The same array can exhibit a behavior of micro- or macroelectrodes. It depends on the scan rates of voltammetric measurement [19]. At very high scan rates the peak-shaped voltammograms indicate linear diffusion within individual microelectrodes, but steady-state behavior is not reached. At very slow scan rates similar non-steady-state peak-shaped voltammograms were observed but linear diffusion is restored due to the overlap of the diffusion layers of individual microelectrodes.

While at very high scan rates the current is proportional to the area of individual microelectrodes, at very slow scan rates it is proportional to the total area of the array [20]. In this case the set of microelectrodes behaves as a single macroelectrode. For intermediate scan rates, the radial diffusion is dominant and thereby voltammograms with a steady-state behavior are recorded. In the range of scan rates from 2 to 500 $mV \cdot s^{-1}$ a sigmoidal response of cyclic voltammograms was found with a steady-state current in the case of lower scan rates (2–10 mV/s), and a peak-shape for higher ones (>100 mV/s) for an array with disc radius of 20 μm [21]. In our case, the behavior of microdisc arrays with disc diameter 2 μm and different interelectrode distance (2 μm and 20 μm) (Fig. 6) was characterized by cyclic voltammetry in 10 mmol/l $K_3Fe(CN)_6$/0.1 $mol \cdot L^{-1}$ KNO_3 solution in a potential range from –1.2 V to +0.6 V vs. Ag/AgCl/Cl^- and scan rates from 10 to 200 $mV \cdot s^{-1}$.

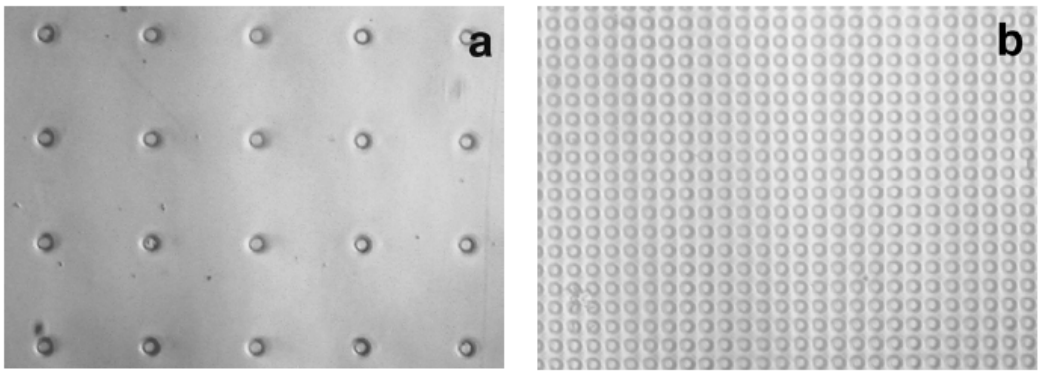

Fig. 6: *Microelectrode array with disc diameter of 2 μm each and interelectrode distance of 20 μm (a) and 2 μm (b).*

According to microelectrode theory, a sigmoidal response was obtained with the microelectrode array (Fig. 7 left) for only the array with interelectrode distance 20 μm, independently of the scan rate in the given range. Compared with a packed microelectrode array, peak-shaped responses were observed with the microelectrode array with interelectrode distance 2 μm (Fig. 7 right) at all scan rates due to the overlap of the diffusion layers of adjacent microdiscs. In the case of the densely spaced interdigitated array electrodes, the microelectrochemical cell consisting of vertically arranged IDA electrodes and continuous Pt film basis with an insulating layer in the middle has been prepared for testing redox cycling by cyclic voltammetry (Fig. 5). The widths of both fingers and gaps were slightly changed (10 μm) and the thickness of the insulating layer (Y_2O_3) was reduced to 250 nm.

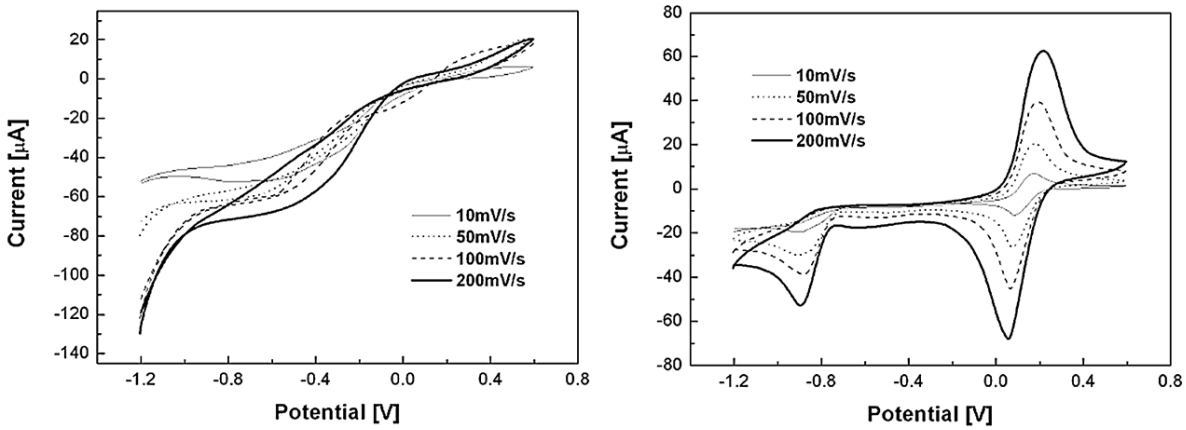

Fig. 7: *Cyclic voltammograms of gold microelectrode array in 0.1 mol/L acetate buffer (pH 4.5) for interelectrode distance of 20 µm (left) and 2 µm (right).*

For the evaluation of cyclic efficiency (current enhancement), the reversible redox couple $[Fe(CN)_6]^{3-}/[Fe(CN)_6]^{4-}$ in aqueous 0.1 M KCl electrolyte was used. Cyclic voltammetry measurements were carried out by a home-built potentiostat unit combined with a simple battery cell potentiometer. In Fig. 8 two voltammograms are shown which were obtained at different voltammetry modes (in single mode or cycling dual-mode). This result demonstrates that the collector current is significantly enhanced (approx. 35 times), when the voltammetry measurement is performed in the redox cycling mode.

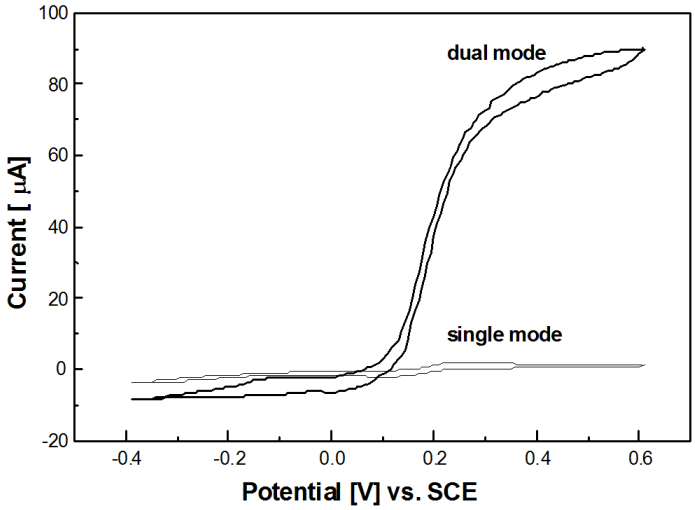

Fig. 8: *The cyclic voltammograms of couple Fe^{2+}/Fe^{3+} in 0.1 M KCl in single and dual-mode set up of vertical IDEA.*

Applications

Mercury Microdisc Array Electrode on Silicon Support

In anodic stripping voltammetry (ASV) with mercury electrodes, it is important to select a supporting electrode material with solubility in mercury as low as possible [22]. The solubility of silicon in mercury is 0.001 %, which is lower than for frequently used metals in this field such as Au, Ag or Pt, but higher than for Ir. For optimum electroplating of mercury, an electrode material with a great potential window is required. In Fig. 9, cyclic voltammograms are shown in acetate buffer (pH 4) recorded for different p- and n-type silicon wafers [23,24]. Intensive hydrogen gas evolution started at approximately –1 V for Si 9218 (n-type) and –1.2 V for Si 9610 (p-type). The quality of a mercury plated microelectrode strongly affects the sensitivity of anodic stripping voltammetry.

Lots of parameters have an influence on the formation of a mercury deposit including plating solution, plating potential and time, etc. In our preliminary experiments we found the optimum concentration of Hg(II) of 1×10^{-3} mol·L^{-1}. Almost no mercury was deposited in the solution with 1×10^{-4} mol·L^{-1} concentration. As far as the plating potential is concerned, a typical value of –1.3 V vs. Ag/AgCl/Cl$^-$ for deposition of mercury on metal or carbon type supports was insufficient for a silicon substrate. We had to combine two deposition steps, the first step at –2 V (for 2 min) followed by the second one at –1.3 V for 2 min.

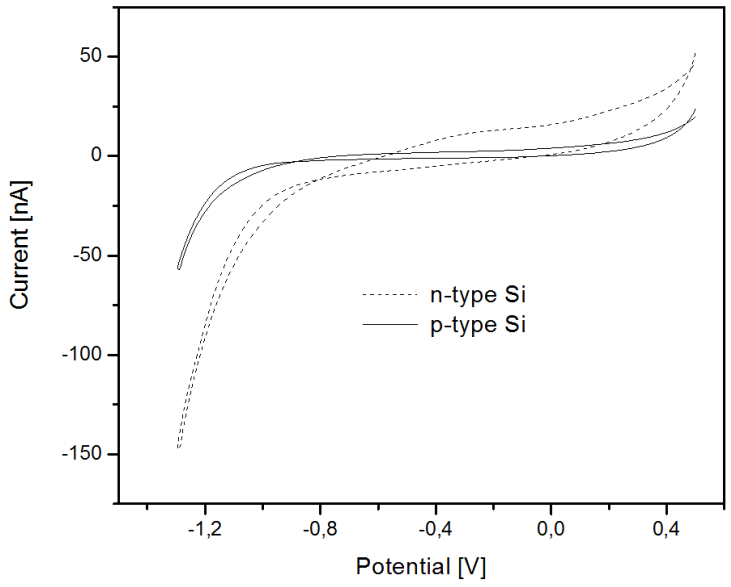

Fig. 9: *The cyclic voltammograms of p- and n-type of silicon wafer in 0.1 M acetate buffer solution.*

We have to note that any attempt to cover the silicon microdisc surface by a true mercury film at a constant deposition potential was not successful. Only typical mercury hemispheres were observed. A detail of mercury hemispheres grown on the silicon microelectrode array is shown in Fig. 10. We have found a strong influence of the electrolyte on mercury plating. We have investigated different electrolytes such as 0.1 $mol \cdot L^{-1}$ acetate buffer (pH 4), 0.1 $mol \cdot L^{-1}$ KNO_3 (acidified by HNO_3 to pH 2.5) and 0.1 $mol \cdot L^{-1}$ $HClO_4$. We also investigated the effect of a small quantity of buffered hydrofluoric acid (BHF) (0.2 %) added to each electrolyte in order to keep the silicon surface without any oxide all the time. It can be concluded that the best mercury hemispheres were formed on p-type of silicon in 0.1 $mol \cdot L^{-1}$ $HClO_4$.

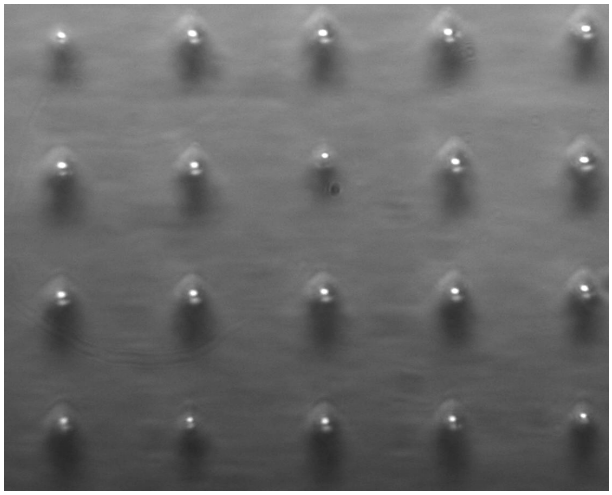

Fig. 10: *Detail of silicon (p-type) microelectrode array preplated by mercury hemispheres.*

In the case of n-type of silicon, the deposit was unstable; most of mercury hemispheres or spheres were moved away from the microelectrodes towards the insulator layer. Usually only a few microelectrodes were covered by mercury. Moreover, no effect of BHF addition on mercury plating was observed. A mercury-plated silicon microelectrode array prepared in a solution of 1×10^{-3} $mol \cdot L^{-1}$ Hg(II) in 0.1 $mol \cdot L^{-1}$ $HClO_4$ with BHF (0.2 %) was used in *ex-situ* determination of Cu(II), Pb(II) and Cd(II). In Fig. 11, the current responses are illustrated of heavy metals with concentration 3.3×10^{-8} $mol \cdot L^{-1}$ using by square wave voltammetry.

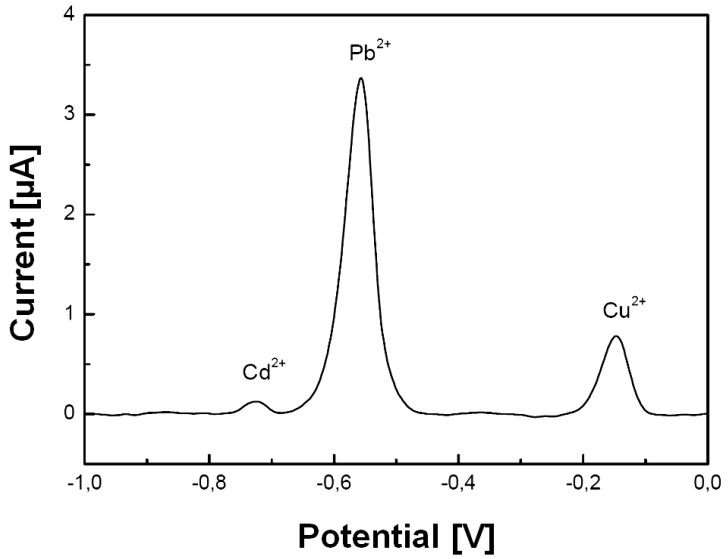

Fig. 11: *Square-wave stripping voltammogram (E_{step} = 5 mV, E_{pulse} = 25 mV and frequency 25 Hz) obtained with silicon microelectrode array in 0.1 mol·L^{-1} KNO_3; preconcentrated at –1 V for 120 s.*

Mercury Microdisc Array Electrode on Nitrogen-Doped DLC Support

In addition, the nitrogen-doped DLC microdisc array was used for *in-situ* simultaneous determination Cu, Pb and Cd by co-deposition of Hg(II), Cu(II), Pb(II), and Cd(II) at –0.8 V in a solution of 1×10^{-4} mol·L^{-1} $Hg(NO_3)_2$ in 0.1 mol·L^{-1} KNO_3 with different contents of heavy metals from 1.6×10^{-8} to 8.3×10^{-8} mol·L^{-1} for 300 s preconcentration time [24,25]. The dependences of current responses on heavy metals concentrations, as well as calibration curves inside are shown in Fig. 12.

As in the previous case, different sensitivities were observed with the mercury-plated microelectrode array to each metal. These differences are probably given by unique properties of the electrodes. This is supported by the fact that all variations of sensitivity were reported for this group of metals [10,26–28]. Addition of a small quantity of SCN^- into the mercury plating solution promoted formation of a mercury film, improved apparently the sensitivity and repeatability of determination of metals. It was concluded that 2×10^{-3} mol·L^{-1} SCN^- is the upper concentration limit because for a higher concentration the mercury surface passivates. Oxidation of mercury to a mercuric ion occurs at a more positive potential (+0.4 V) than that for the formation of the thiocyanate complex. Anyway, the stripping current for Pb was increased 10 times in comparison with that in the absence of thiocyanate.

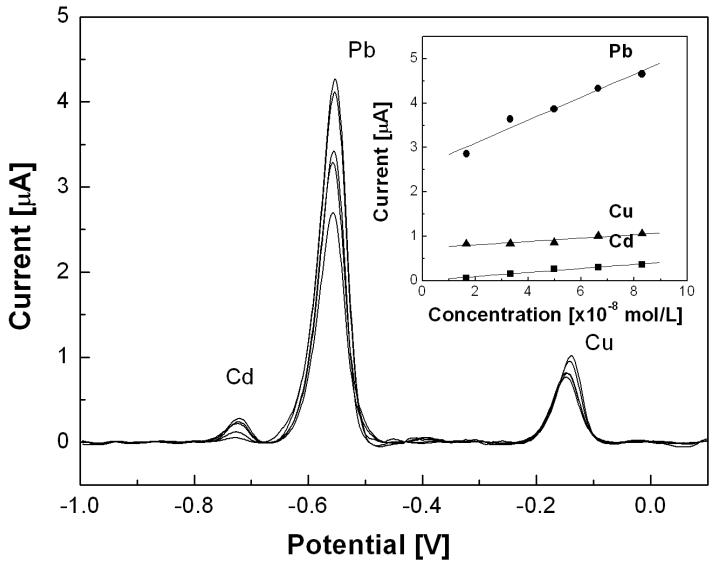

Fig. 12: *Differential pulse stripping voltammograms (E_{step} = 2 mV, E_{pulse} = 50 mV, 25 ms pulse and 30 mV scan rate). Dependence of current response of nitrogen-doped DLC-Hg microelectrode array on concentration of metals with calibration curve inside; preconcentration time: 300 s.*

Bismuth Microdisc Array Electrode on Nitrogen-Doped DLC and Boron-Doped Diamond Supports

Excellent performance of ASV with bismuth film electrodes (BiFEs) in determination of Pb(II), Cd(II), and Zn(II) on various carbon substrates had already been demonstrated [29–33]. BiFEs on nitrogen-doped DLC microelectrode arrays for *in-situ* determination of Pb(II) were prepared by co-deposition of Bi(III) and Pb(II) at –1.3 V vs. Ag/AgCl/Cl^- in a plating solution of $Bi(NO_3)_3$ in a supporting electrolyte (0.1 mol·L^{-1} acidified KNO_3 (pH 2)) with different contents of Pb(II) [24,34,35]. For the ASV experiments, concentrations of 2.5×10^{-6} or 5×10^{-6} mol·L^{-1} were chosen because the stripping current was not increased at higher concentration of Bi than 5×10^{-6} mol·L^{-1} and, moreover, the bismuth peak shape was deformed.

We have found a minimum effect of different supporting electrolytes (0.1 mol/L acetate (pH 4), nitrate (acidified by HNO_3) or perchlorate solutions) in the bismuth plating procedure. The deposit of the bismuth film was investigated by SEM (Fig. 13). Different morphologies of the bismuth structure on NDDLC and BDD prepared under the same

conditions can be seen. The dependence of voltammetric response of bismuth-plated NDDLC array to Pb(II) concentration is shown in Fig. 14.

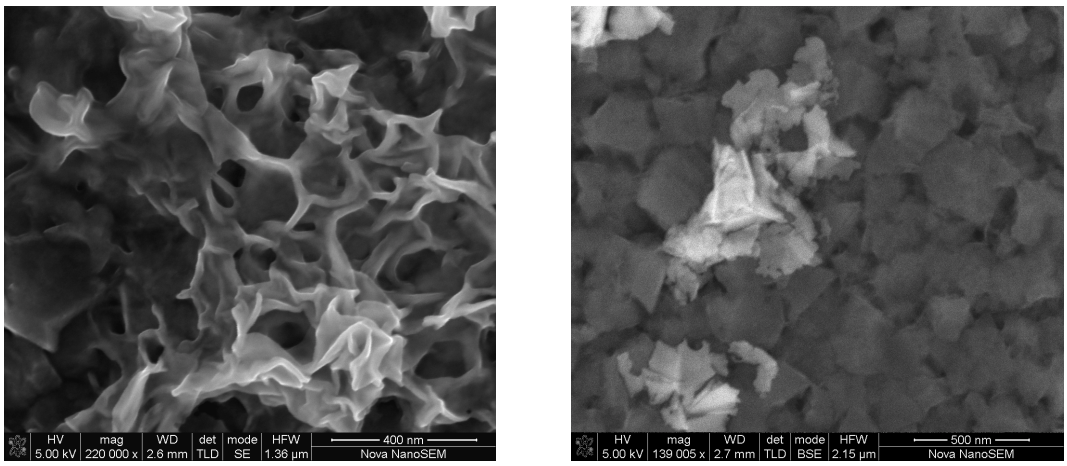

Fig. 13: *SEM image of bismuth film deposit prepared at −1.3 V for 120 s in 0.1 mol·L^{-1} acetate buffer with 4x10^{-5} mol·L^{-1} of Bi^{3+} on NDDLC (left) and BDD (right).*

The stripping current was linear in the range from 2×10^{-8} to 1.2×10^{-7} mol·L^{-1} concentration of Pb(II) with a sensitivity of 2.5µAL/µmol. In the case of BDD on silicon support, the effect of a different content of boron on the performance of bismuth film MAEs in determination of Zn, Cd and Pb was investigated [36].

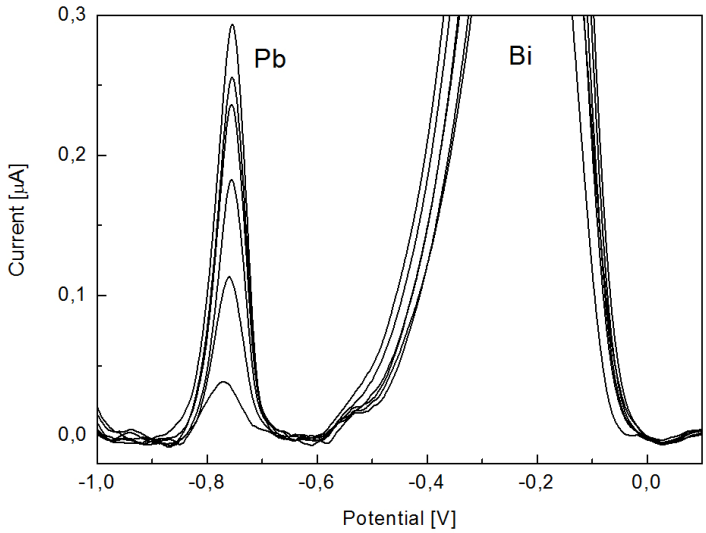

Fig. 14: *Differential pulse stripping voltammograms (E_{step} = 2 mV, E_{pulse} = 50 mV, 25 ms pulse and 30 mV scan rate). Dependence of current response of nitrogen-doped DLC-Bi*

microelectrode array on Pb(II) concentration in 0.1 mol·L^{-1} KNO_3 (pH 2); preconcentration time: 120 s.

In Fig. 15 (left), the voltammograms are compared recorded under the same conditions (concentration of each of metals was 6×10^{-8} mol·L^{-1}). The responses which are obtained for BDD (6000 ppm of B:C) were lower than for BDD (10000 ppm B:C) and their peaks were slightly shifted and not so sharp. Probably the higher concentration of boron in the film increased the electrical conductivity of the film and thus the conditions for electroplating the bismuth layer could be better. In the next Fig. 15 (right), the square wave voltammograms of Zn, Cd and Pb are shown in concentration range from 2×10^{-8} to 1×10^{-7} mol·L^{-1}.

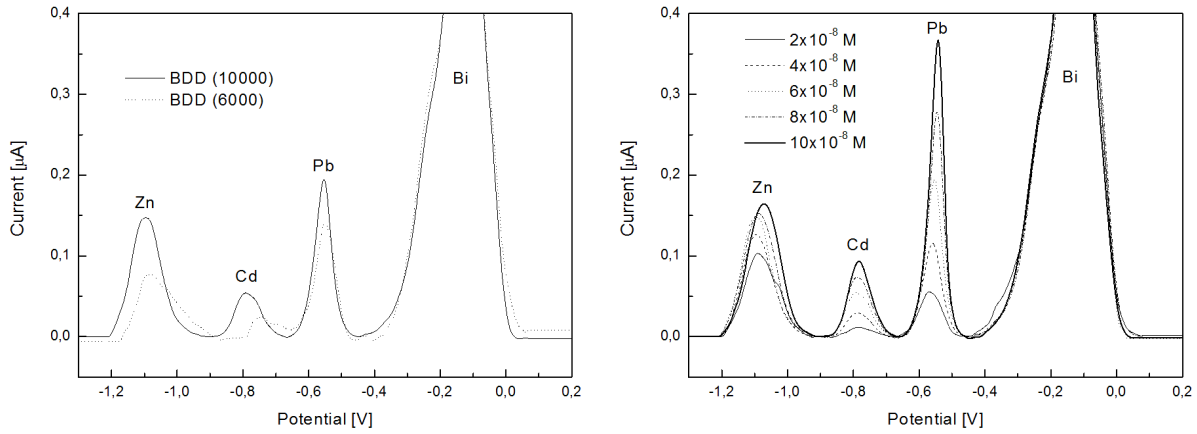

Fig. 15: *Square-wave stripping voltammograms (E_{step} = 8 mV, E_{pulse} = 25 mV and frequency 50 Hz). Dependence of current responses of BDD microelectrode array with different contend of boron (left) on concentration of metals (6x10^{-8} mol/L of each) and BDD microelectrode array (for B:C ratio 10 000 ppm in the gas phase) on concentration of metals (right); preconcentration time: 120 s.*

Platinum interdigitated array electrode (IDAE) on silicon/silicon dioxide support

IDAEs were used for real sample analysis of trace concentration of iron in rods of ultrapure spectral carbon by substitutional stripping voltammetry [37]. Preliminary experiments with synthetic samples of iron in the concentration range from 3×10^{-7} to 6×10^{-6} M proved that determination of Fe can be performed well thanks to the enhanced current by redox cycling at the IDAEs. Since the required limiting level of Fe for real spectral carbon was 0.5×10^{-4} % (m/m) in all but one sample, the content of Fe was below this purity level. No significant differences in determination were observed in comparison with the results obtained by atomic

absorption spectrometry (AAS) and, therefore, the electrochemical method applying IDAEs can be considered as a cheaper alternative.

The same vertically arranged IDAE was applied in voltammetric determination of selenium in environmental water [38]. In comparison with other methods (voltammetry at hanging mercury drop electrode and gold rotating disc electrode), this method provided the most reliable and reproducible results over the investigated concentration range from 2 to 40 $\mu g \cdot L^{-1}$. By the method of standard addition, the concentrations of Se in range of 1.8–2.5, 4.5–6.2 and 1.0 $\mu g \cdot L^{-1}$ were found in tap, river and spring water, respectively.

Conclusions

Voltammetric analysis at microfabricated microelectrode has been proven to be very promising. The small size, high sensitivity, low limit of detection as well as high reproducibility and fast responses are the main benefits of MEAs. In addition, MEAs are suitable for electrochemical analysis in non-polar solvents or low-conductive electrolytes. This review includes, in addition to theoretical aspects of the MEs and MEAs with loosely and densely spaced electrodes, also their fabrication processes and their electrochemical characterization. As for fabrication, the photolithographic method becomes increasingly important for the development of microelectrode arrays of various geometries for the use in a wide variety of analytical problems. In this paper, our attention is focused on microdisc electrode arrays and interdigitated array electrodes. Finally, selected examples are presented of the application of MEAs in environmental analysis.

Acknowledgements

This work was supported by the Scientific Grant Agency of the Ministry of Education of the Slovak Republic and the Slovak Academy of Sciences, Nos. 1/1106/12, 1/1102/11 and 1/1103/11 and by the Slovak Research and Development Agency under contract Nos. APVV-0199-10 and LPP-0094-09.

References

1. J. Orozco, C. Fernandez-Sanchez, C. Jimenez-Jorquera: *Sensors **10*** (2010) 475.
2. R. Feeney, S.P. Kounaves: *Electroanalysis **12*** (2000) 677.

3. R.J. Forster, Tia E. Keyes; in: *Handbook of Electrochemistry* (C.G. Zoski Ed.), p. 155. Elsevier, Amsterdam, 2007.
4. J. Wang: *Analytical electrochemistry,* 2nd Ed. pp. 149–163. John Wiley and Sons, New York, 2000.
5. K. Aoki: *Electroanalysis* ***5*** (1993) 627.
6. J. Heize: Angew. Chem. Int. Ed. Engl. **32** (1993) 1268.
7. S.P. Kounaves, W. Deng: *Anal. Chem.****65*** (1993) 375.
8. K. Stulik, C. Amatore, K. Holub, W. Kutner: *Pure Apl. Chem. **72*** (2000) 1483.
9. K. Aoki, J. Osteryoung: *J. Electroanal. Chem. **122*** (1981) 19.
10. X. Xie, D. Stuben, Z. Berner, J. Albers, R. Hintsche, E. Jentzen: *Sens. Actuators **B97 (***2004) 168.
11. C. Belmont, M.L. Tercier, J. Buffle, G.C. Fiaccabrino, M. Koudelka-Hep: *Anal. Chim. Acta **329*** (1996) 203.
12. S.P. Kounaves, W. Deng, P.R. Hallock, G.T.A. Kovacs, C.W. Storment: *Anal. Chem. **66*** (1994) 418.
13. A.E. Cohen, R.R. Kunz: *Sensors and Actuators **B62*** (2000) 23.
14. M. Paeschke, U. Wollenberger, T. Lisec, U. Schnakenberg, R. Hintsche: *Sensors and Actuators **B26–27*** (1995) 394.
15. Y. Iwasaki, M. Morita: *Current Separations **14:1*** (1995) 2.
16. O. Niwa, M. Morita, H. Tabei: *J. Electroanal. Chem. **262*** (1989) 291.
17. A.J. Bard, J.A. Crayston, G.P. Kittlesen, T. Varco Shea, M.S. Wrighton: *Anal. Chem. **58*** (1986) 2321.
18. K. Aoki, M. Morita, O. Niwa, H. Tabei: *J. Electroanal. Chem. **256*** (1988) 269.
19. H.P. Wu: *Anal. Chem. 65* (1993) 1643.
20. C. Amatore: *Physical electrochemistry,* pp. 131–208. Marcel Dekker, New York, 1995.
21. S.P. Kounaves, W. Deng: *J. Electroanal. Chem. **301*** (1991) 77.
22. S.P. Kounaves: *Thesis No. 2151,* 1985.
23. V. Rehacek, I. Hotovy, L. Spiess, M. Gubisch; at: *51st Internationales Wissenschaftliches Kolloquium, Technische Universitat Ilmenau,* Ilmenau (Germany) September 11–15, 2006.
24. V. Rehacek, I. Hotovy; in: *Heavy Metal Pollution* (S.E. Brown, W.C. Welton, Eds.), p. 327. Nova Science Publishers, Inc., New York, 2008.
25. V. Rehacek, I. Hotovy, M. Vojs: *Journal of Physics: Conference Seri*es ***61*** (2007) 982.
26. A. Uhlik, M. Paeschke, U. Schnakenberg, R. Hintsche, H.J. Diederich, F. Scholz: *Sensors and Actuators **B24–25*** (1995) 899.
27. P.R.M. Silva, M.A. El Khakani, M. Chaker, A. Dufresne, F. Courchesne: *Sensors and Actuators **B76*** (2001) 250.
28. P.R.M. Silva, M.A. El Khakani, M. Chaker, G.Y. Champagne, J. Chevalet, L. Gastonguay, R. Lacasse, M. Ladouceur: *Anal. Chim. Acta **385*** (1999) 249.
29. A. Economou: Trends in Analytical Chemistry **24** (2005) 334.
30. J. Wang, J. Lu, U.A. Kirgoz, S.B. Hocevar, B. Ogorevc: *Anal. Chim. Acta **434*** (2001) 29.
31. J. Wang, J. Lu, S.B. Hocevar, P.A.M. Farias: *Anal. Chem.**72*** (2000) 3218.

32. J. Wang: *Electroanalysis **17*** (2005) 1341.
33. I. Svancara, L. Baldrianova, E. Tesarova, S.B. Hocevar, S.A.A. Elsuccary, A. Economou, S. Sotiropoulos, B. Ogorevc, K. Vytras: *Electroanalysis **18*** (2006) 177.
34. V. Rehacek, I. Hotovy, M. Vojs, F. Mika: *Microsystem Technologies **14*** (2008) 491.
35. V. Rehacek, I. Hotovy, M. Vojs: *Sensors and Actuators **B127*** (2007) 193.
36. M. Vojs, E. Sipos, V. Rehacek, M. Marton, M. Varga, M. Vesely; at: *APCOM 2010: 16th International Conference.* Malá Lučivná (Slovak Republic); 16.–18.6. 2010.
37. D. Bustin, S. Mesaros, P. Tomcik, M. Rievaj, V. Tvarozek: *Analytica Chimica Acta **305*** (1995) 121.
38. M. Rievaj, J. Mocak, D. Bustin: *Chem. Anal. **44*** (1999) 1025.